Intelligent Load Frequency Control in Multi-Area Power Systems through Brain Emotional Learning

M. Nakhaeemoghaddam*, S. Khorashadizadeh, R. Shariatinasab

Abstract-- In conventional control techniques based on power system linearization around a given point, outputs are dissatisfactory under sudden variations in load and displacement of the working point. Therefore, several methods have been introduced to adapt such controllers to variations in system operations. This paper proposes an intelligent load frequency control (LFC) technique for multi-area power systems with an emotional neural network (ENN), the parameters of which are tuned through the bird swarm algorithm (BSA). The proposed emotional learning-based intelligent controller is inspired by the mammalian brain limbic system in light of its effectiveness and efficiency in control applications. Simulations were performed in MATLAB on an intrinsically nonlinear three-area power system under sudden load and parameter changes. The proposed model was compared to classical proportional–integral–derivative (PID), standard ENN, and indirect adaptive fuzzy controllers under various operating conditions and parameter changes. According to the results, the proposed methodology was faster and more accurate in controlling frequency variations and power transfer changes between power system areas. The main novelty of this work lies in the integration of a continuous radial basis emotional neural network (CRBENN) with a Lyapunov-based direct adaptive robust control framework (DARENC), optimized via Bird Swarm Algorithm (BSA), for load frequency control in multi-area power systems under uncertainties. The key novelty of this work lies in the integration of a continuous radial basis emotional neural network (CRBENN) with a Lyapunov-based direct adaptive robust control framework (DARENC), optimized via Bird Swarm Algorithm (BSA), for load frequency control in multi-area power systems under uncertainties.

Keywords: load frequency control, multi-area power systems, brain emotional learning.

I. Introduction

A large-scale power system has a few control areas, each of which has a number of generators. The control areas are interconnected through connection lines. Each control area has primary and complementary control measures. Primary control measures provide steady-state frequency deviation for system load alternation, depending on the governor droop characteristics and load frequency sensitivity. The restoration of the system to the nominal frequency requires a complementary control measure to adjust the load reference point through the motor. As a result, the control of the reference adjustment points of the selected generation units is the main power control stimulus to adapt to system load changes [1]. A load frequency controller (LFC) is mainly intended to adjust the system frequency to a predefined nominal value and maintain the exchanged power between control areas at the programmed levels. Earlier works studied different LFC schemes [2]. Many controllers have been proposed for LFC problems to obtain satisfactory dynamic performance. Constant-gain controllers such as proportional-integral (PI) and proportional-integral-derivative (PID) are widely used. A novel control structure with a tuning method was introduced to design a PID–LFC for power systems. The implementation of LFC requires accurate information on the parameters of control areas, which are often inaccurately modeled or change due to aged components. Therefore, intelligent control techniques have been adopted.

"Recently, brain emotional learning (BEL) has emerged as a promising intelligent approach for LFC. Barik and Das (2022) applied a BEL-based controller for microgrid frequency regulation [19], while Kheradmandi et al. (2020) developed an improved BEL algorithm for robust LFC [20]. A comprehensive review of BEL-based frequency control was provided by Liu et al. (2022) [21]. Additionally, Abd-Elazim and Ali (2022) utilized Henry gas solubility optimization for multi-area LFC [18]." Among these intelligent techniques, e.g., fuzzy systems, artificial neural networks (ANNs), and genetic algorithms (GA), have been of increasing interest to researchers over the past two decades to cope with several aspects of power systems [5]. Earlier works studied the generator adaptive fuzzy output tracking stimulus control of power systems [6]. An integrated fuzzy gain scheduled controller was introduced for the LFC of two-area power systems [7]. An ANFIS-based control scheme was proposed for the optimization and updating of control achievements for

Manuscript received 25 November 2025; revised 15 December 2025; accepted 26 May 2026.

Digital Object Identifier 10.22077/ijpe.2026.10576.1032

M. Nakhaeemoghaddam PhD student at Department of Electrical Engineering, Iran, University of Birjand , Birjand, Iran (e-mail: mob.nakhaee74@gmail.com).

S. Khorashadizadeh Associate Professor at Faculty of Electrical and Computer Engineering, University of Birjand , Birjand, Iran (e-mail: s.khorashadizadeh@birjand.ac.ir).

R. Shariatinasab Professor at Faculty of Electrical and Computer Engineering, University of Birjand , Birjand, Iran (e-mail: shariatinasab@birjand.ac.ir).

automatic generation control (AGC) based on load changes [8]. A fuzzy system was employed for the adaptive termination of proportional and integral advantages of a PI controller based on the area control error and its change for LFC [9]. An LFC was developed for power systems, provided that the system would be nonlinear in the valve position and have parametric uncertainty, using the Takagi–Sugeno (T–S) fuzzy system [10]. Earlier studies proposed a model for type-2 fuzzy systems for the LFC of an interconnected two-area thermal recovery system consisting of superconducting magnetic energy storage (SMES) units [11]. Moreover, a GA-based fuzzy gain scheduling approach was introduced for LFC [12]. Researchers proposed two strong decentralized control design techniques for LFC using linear matrix equations and GA optimization [13]. The bacteria foraging optimization algorithm (BFOA) was used to search the optimal parameters of PID controllers to minimize the time-domain objective function [14]. A decentralized predictive LFC was developed for multi-area power systems [15, 16].

This paper consists of different sections. Section 2 describes the dynamic model of the multi-area power system, in which the dynamic model of each area, LFC model, and the state space model of the system are provided. Section 3 proposes the continuous radial basis emotional neural network (CRBENN). Section 4 analyzes the proposed CRBENN model and provides the simulation results by using particle swarm optimization (PSO) for the coefficient optimization of PID, standard emotional, and CRBENN controllers, comparing the three controllers to each other and to the reference. Finally, Section 5 draws a research conclusion and provides future research suggestions.

II. DYNAMIC MODEL OF MULTI-AREA POWER SYSTEM

Figure 1 demonstrates a schematic view of a power system consisting of N LFC areas. Each area has a number of generators. The generators of a given area are simplified in the form of a single generator [1]. Each area is also assumed to have gas turbines with simple and combined cycles and heat recovery steam turbines. The proposed controller is installed on the gas turbines, whereas the steam turbines have no control at the reference adjustment point. The dynamic model of an area can be written as:

$$\Delta\dot{f}_i = \frac{1}{M_i}\left(-D_i\Delta f_i + \Delta p_{t1i} + \Delta p_{t2i} - \Delta p_{di}\right) \tag{1}$$

$$\Delta\dot{P}_{t1i} = \frac{1}{T_{t1i}}\left(-\Delta P_{t1i} + \Delta P_{g1i}\right) \tag{2}$$

$$\Delta\dot{P}_{t2i} = \frac{1}{T_{t2i}}\left(-\Delta P_{t2i} + \Delta P_{g2i}\right) \tag{3}$$

$$\Delta\dot{P}_{g1i} = \frac{1}{T_{g1i}}\left(-\Delta P_{g1i} + u_i - \frac{\Delta f_i}{R_i}\right) \tag{4}$$

$$\Delta\dot{P}_{ri} = \frac{1}{T_{ri}}\left(-\Delta P_{ri} + \left(1 - \frac{K_{ri}T_{ri}}{T_{g2i}}\right)\Delta P_{g2i} + \frac{K_{ri}T_{ri}}{T_{g2i}}\left(\Delta\bar{r}_i - \frac{\Delta f_i}{R_i}\right)\right) \tag{5}$$

$$\Delta\dot{P}_{g2i} = \frac{1}{T_{g2i}}\left(-\Delta P_{g2i} + \Delta\bar{r}_i - \frac{\Delta f_i}{R_i}\right) \tag{6}$$

$$\Delta\dot{P}_{tiei} = \frac{1}{2\pi}\left(\sum_{\substack{j=1\\ j\neq i}}^{N} T_{ij}\,\Delta f_i - \sum_{\substack{j=1\\ j\neq i}}^{N} T_{ij}\,\Delta f_i\right) \tag{7}$$

Figure 2 depicts the block diagram of an LFC area in a multi-area power system. Drawing on a state space representation, Eqs. (1-7) can be rewritten in a compact form:

$$\dot{\bar{X}}_i = \bar{A}_{ii}\bar{X}_i + \bar{B}_i\bar{u}_i + \bar{E}_i\Delta\bar{r}_i + \sum_{\substack{j=1\\ j\neq i}}^{N} \bar{A}_{ij}\,\bar{X}_j - \bar{F}_i\Delta P_{di} \tag{8}$$

$$y_i = \bar{C}_i\bar{X}_i \tag{9}$$

Where the state vector and control area matrices are defined as:

$$\overline{X_i} = \begin{bmatrix} \Delta f_i & \Delta P_{t1i} & \Delta P_{g1i} & \Delta P_{t2i} & \Delta P_{ri} & \Delta P_{g2i} & \Delta P_{tiei} \end{bmatrix}^T \tag{10}$$

$$\overline{A_{ij}} = \begin{bmatrix} 0 & 0 & 0 & 0 & 0 & 0 & 0 \\ 0 & 0 & 0 & 0 & 0 & 0 & 0 \\ 0 & 0 & 0 & 0 & 0 & 0 & 0 \\ 0 & 0 & 0 & 0 & 0 & 0 & 0 \\ 0 & 0 & 0 & 0 & 0 & 0 & 0 \\ 0 & 0 & 0 & 0 & 0 & 0 & 0 \\ -2\pi T_{ij} & 0 & 0 & 0 & 0 & 0 & 0 \end{bmatrix} \tag{11}$$

$$\overline{B_i} = \begin{bmatrix} 0 & 0 & \frac{1}{T_{g1i}} & 0 & 0 & 0 & 0 \end{bmatrix}^T$$

$$\overline{A_i} = \begin{bmatrix} \frac{-D_i}{M_i} & \frac{1}{M_i} & 0 & \frac{1}{M_i} & 0 & 0 & -\frac{1}{M_i} \\ 0 & -\frac{1}{T_{t1i}} & \frac{1}{T_{t1i}} & 0 & 0 & 0 & 0 \\ -\frac{1}{R_iT_{g1i}} & 0 & -\frac{1}{T_{g1i}} & 0 & 0 & 0 & 0 \\ 0 & 0 & 0 & -\frac{1}{T_{t2i}} & \frac{1}{T_{t2i}} & 0 & 0 \\ -\frac{K_{ri}}{R_iT_{g2i}} & 0 & 0 & 0 & -\frac{1}{T_{g2i}} & \frac{-1}{T_{ri}}\left(\frac{-K_{ri}}{T_{g2i}} + \frac{1}{T_{ri}}\right) & 0 \\ -\frac{1}{R_iT_{g2i}} & 0 & 0 & 0 & 0 & -\frac{1}{T_{g2i}} & 0 \\ \sum\limits_{j=1, j\neq i}^{N} 2\pi T_{ij} & 0 & 0 & 0 & 0 & 0 & 0 \end{bmatrix} \tag{12}$$

$$\overline{F_i} = \begin{bmatrix} \frac{1}{M_i} & 0 & 0 & 0 & 0 & 0 & 0 \end{bmatrix}^T \tag{13}$$

$$\overline{E_i} = \begin{bmatrix} 0 & 0 & 0 & \frac{K_{ri}}{T_{g2i}} & \frac{1}{T_{g2i}} & 0 & 0 \end{bmatrix}^T \tag{14}$$

$$\overline{C_i} = \begin{bmatrix} 1 & 0 & 0 & 0 & 0 & 0 & 0 \end{bmatrix} \tag{15}$$

Where $\Delta\overline{r_i}$ is the change in the steam turbine adjustment reference point (assumed to be zero), ΔP_{di} is the load change, and $T_{ij} = T_{ji}$.

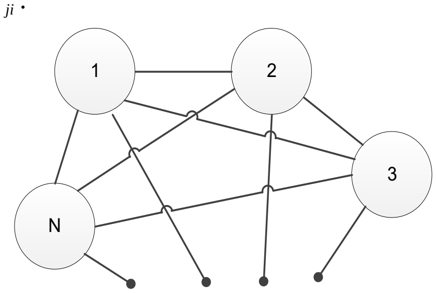

Fig. 1. Schematic view of an N-area power system

To simplify the design of the controller, Eqs. (8) and (9) are converted into conventional controllers:

$$\dot{X}_i = A_{ii}X_i + B_iu_i + \sum_{\substack{j=1\\ j\neq i}}^{N} A_{ij}X_j - F_i\Delta P_{di} \tag{16}$$

$$y_i = C_iX_i \tag{17}$$

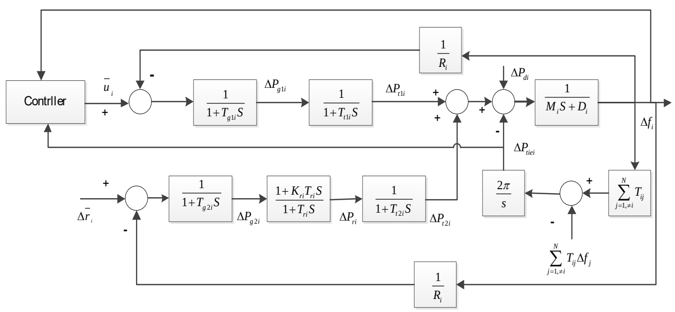

Fig. 1. Dynamic model of the ith area in a multi-area power system.

The parameters of Eqs. (11-18) are obtained as:

$$\begin{aligned} A_{ii} &= S_i^{-1}\overline{A_{ii}}S_i, A_{ij} = S_i^{-1}\overline{A_{ij}}S_j \\ B_i &= S_i^{-1}\overline{B_i}, F_i = S_i^{-1}\overline{F_i}, C_i = \overline{C_i}S_i \end{aligned} \tag{18}$$

Where S_k is the similarity transformation matrix [3].

The isolated and undisturbed LFC area is obtained as:

$$\dot{X}_i = A_{ii}X_i + B_iu_i \tag{19}$$

The transformed matrices A_{ii}, B_i and C_i are given by [4]:

$$\overline{A_{ii}} = \begin{bmatrix} 0 & 1 & 0 & 0 & 0 & 0 & 0 \\ 0 & 0 & 1 & 0 & 0 & 0 & 0 \\ 0 & 0 & 0 & 1 & 0 & 0 & 0 \\ 0 & 0 & 0 & 0 & 1 & 0 & 0 \\ 0 & 0 & 0 & 0 & 0 & 1 & 0 \\ 0 & 0 & 0 & 0 & 0 & 0 & 1 \\ -a_{0i} & -a_{1i} & -a_{2i} & -a_{3i} & -a_{4i} & -a_{5i} & -a_{6i} \end{bmatrix} \tag{20}$$

$$\overline{B_i} = \begin{bmatrix} 0 \\ 0 \\ 0 \\ 0 \\ 0 \\ 0 \\ 1 \end{bmatrix}, \overline{C_i} = \begin{bmatrix} c_{0i} & c_{1i} & c_{2i} & c_{3i} & c_{4i} & 0 & 0 \end{bmatrix} \tag{21}$$

The last row of matrix $\overline{A_{ii}}$ is denoted as $-a_{ji}$, i=1,…, N, and j=0, …, 6. The parameters are dependent on the system, and their calculation is described in [5].

For $C_{ki}>0$, k=0,…4, it can be proved that each local area given by Eq. (19) has a relative degree of 3 and zero dynamic stability. The continuous integration of Eq. (17) and the use of Eq. (19) until the appearance of the input yield:

$$y_i = C_iA_{ii}^3X_i + c_{4i}u_i, c_{4i} \neq 0 \tag{22}$$

Once the parameters of Eq. (17) and (18) have been accurately found, ideal local control u_i^* is given by:

$$u_i^* = \frac{1}{c_{4i}}\left(y_{mi} + K_i^Te_i - C_iA_{ii}^3X_i\right) \tag{23}$$

Where y_{mi} is a given reference signal. The derivatives are assumed to be constrained (to 3). For tracking error definition of $e_i = y_{mi} - y_i$ the control rule in Eq. (23) makes the error vector $e_i = \begin{bmatrix} e_i & e^{\bullet}_i & e^{\bullet\bullet}_i \end{bmatrix}^T$ converge to zero, provided that $K_i = \begin{bmatrix} K_{0i} & K_{1i} & K_{2i} \end{bmatrix}^T$ is selected such that all the roots of the following characteristic equation are in the left-side open half of the plane:

$$S^3 + K_{2i}S^2 + K_{1i}S + K_{0i} = 0 \tag{24}$$

In the presence of unknown subsystem parameters, a local controller [15] cannot be designed accurately. To obtain accurate tracking for an interconnected system [14] with unknown parameters, a CRBENN was developed, as described below.

III. CRBENN

The CRBENN has basic functions in thalamus nodes; however, there is no direct connection between the thalamus and amygdala. Therefore, the CRBENN is obtained through simple manipulation of radial basis function (RBF) networks with additional characteristics from emotional models due to the amygdala component and its non-reducing weights. Thus, its universal approximation characteristic is simply proved based on RBF network features. Hence, the CRBENN uses the characteristics of RBF networks, e.g., universal approximation, continuity, and derivability based on the weights. It is also demonstrated that the universal approximation proof for the CRBENN is generalizable, and any symmetric RBF kernel can be assumed as thalamus nodes. Then, the CRBENN is employed in a direct adaptive control structure to directly estimate the control input. The general stability of the emotion-based controller is ensured based on Lyapunov stability, which is an important aspect of the proposed controller. This theoretical conclusion has been reported in some emotion-based controller papers with specific considerations and simplifications. Furthermore, the update rules are consistent with the main emotional mind models; i.e., they meet the need for non-reducing amygdala weights.

Overall, the novelty of the proposed model includes:

1) The CRBENN provides simple and continuous mapping with universal approximation. Hence, it can be applied to different control engineering problems as a general computational framework. It should be mentioned that universal approximation is an essential mathematical characteristic that represents the proposed computational frameworks in the same class of approaches as polynomials and Fourier series [5]. For a level of collaboration, the study of Hornik et al. (1989) on neural networks and the study of Castro (1995) on fuzzy systems may be cited.
2) The CRBEEN is used in a direct adaptive control framework for a class of unknown nonlinear systems, and general structure stability has been proved using

Lyapunov stability without deviation from the basic emotional brain rules [5].

This section describes the CRBENN model and evaluates its universal approximation using the universal approximation property of RBF networks.

A. CRBENN Configuration

Figure 3 illustrates the CRBENN configuration. Evidently, the CRBENN is generally similar to brain emotional learning (BEL)-based models such as BELBIC [8]. However, the CRBENN has three major characteristics. Firstly, there is no direct connection between the thalamus and amygdala. Earlier works held that a direct thalamus-amygdala connection would interfere with normal learning and yield undesirable outcomes in simulation [9]. The elimination of such a direct connection leads to a smooth, continuous CRBEEN output. Secondly, each thalamus node is an RBF [5]. This is similar to earlier works [10]. However, it is different from [11] and BELBIC [8], where the thalamus was a simple identity function. A combined effect of these two characteristics results in universal approximation as the third characteristic.

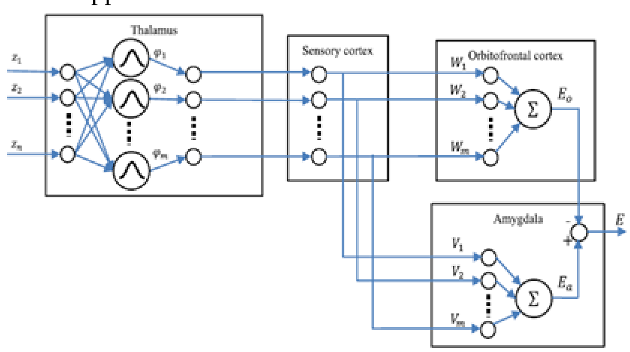

Fig. 3. CRBENN configuration

Moreover, the universal approximation proof of the CRBENN is general; hence, any symmetric RBF kernel can be considered in the thalamus nodes (which is discussed in the next section). Here, Gaussian functions are a major type of RBFs [5]. Once the input has been introduced to the thalamus, RBFs are generated as [5]:

$$\varphi_j = \exp\left(-\left[\frac{\left(z-\mu_j\right)^T-\left(z-\mu_j\right)}{\sigma_j^2}\right]\right) \tag{25}$$

Where $z=[z_1,\ldots,z_n]^T \epsilon R^n$ is the general input sensing vector, $\mu_j \epsilon R^n$ is the average factor, $\sigma_j>0$ is the smoothing factor, and m is the total number of nodes. The CRBENN has the universal approximation property and can approximate any nonlinear function using a sufficiently large m value [5].

Therefore, the input sensing RBF vector is the output of the thalamus. This vector is then introduced to the amygdala and orbitofrontal cortex (OFC) through the sensory cortex, and the outputs are obtained as [5]:

$$E_a = \sum_{j=1}^{m} V_j \varphi_j = V^T \varphi \tag{26}$$

$$E_0 = \sum_{j=1}^{m} \omega_j \varphi_j = \omega^T \varphi \tag{27}$$

Where V_j and W_j (j=1, …, m) denote the weights of the amygdala and OFC nodes, respectively. Here, the weight vectors, $V=[V_1,V_2,\ldots,V_m]^T \in R^m$, $W=[w_1,w_2,\ldots,w_m]^T \in R^m$, and $\varphi=[\varphi_1,\varphi_2,\ldots,\varphi_m]^T \in R^m$ are RBF vectors. According to Eqs. (26) and (27), the number of nodes in the thalamus is equal to the total nodes of the amygdala and OFC [5].

According to Fig. 3, the model output is calculated by subtracting the OFC output from the amygdala output:

$$E = E_a - E_0 = \sum_{j=1}^{m} V_j \varphi_j - \sum_{j=1}^{m} \omega_j \varphi_j = \left(V-\omega\right)^T \varphi \tag{28}$$

This section introduced the CRBENN architecture. The universal approximation proof of the CRBENN is provided in [5]. An adaptive control structure and update rules for the amygdala and OFC node weights are designed in agreement with Moren's model below [11]. Moreover, in the control structure of [5], RBF parameters in the thalamus, i.e., μ_j and σ_j, are constant for simplifications, and the number of adaptive parameters was reduced. In related simulations, RBF centers have the same distance in the input range, and the same smoothing factor is applied to all the nodes.

B. Problem Formulation

Based on Eq. (19), the derivative of the last state variable can be rewritten as:

$$x^{(n)} = f\left(\underline{x}\right) + g\left(\underline{x}\right)u + d\left(\underline{x},t\right) \tag{29}$$

Where f(x) and g(x) could be calculated through the matrices defined in Eqs. (20) and (21), $\underline{x} = [x, \dot{x}, \ldots\ldots, x^{(n-1)}]^T \in R^n$ denotes the state vector, u is the control input, $d(\underline{x},t)$ denotes disturbance with upper bound $\left\|d\left(\underline{x},t\right)\right\| \le \varepsilon_d$, $f\left(\underline{x}\right)$, which is an unknown function that meets $\left\|f\left(\underline{x}\right)\right\| \le f_1 < \infty$ for any $\underline{x}$ in the controllable area $U \subset R^n$. When f_1 is an unknown constant, $g\left(\underline{x}\right)$ is a smooth function that is met by $0 < g\left(\underline{x}\right) \le g_1 < \infty$ and $g_1 > 0$ as the upper bound [5]. Some studies designed direct adaptive controllers with unknown $g\left(\underline{x}\right)$ [12-14]. The tracking error is defined as:

$$e = x_d - x \tag{30}$$

Where x_d is the desired value. It is assumed that x_d and its derivatives are constrained to the n-order derivative. The error function s is defined as [5]:

$$s = e^{(n-1)} + \Lambda_{n-1} e^{(n-2)} + \cdots + \Lambda_1 e \tag{31}$$

Where $\Lambda_k \left(k=1,\ldots,n-1\right)$ is a positive constant. The differentiation of Eq. (31) with respect to time yields; Where $q_a = x_d^{(n)} + \Lambda_{n-1} e^{(n-1)} + \cdots + \Lambda_1 \dot{e}$. This study aimed to design a direct adaptive control structure such that the tracking error converges to zero, and all the signals are constrained while the approximation error and external disturbance effects are kept below the desired damping level [5].

$$\dot{s} = -f(\underline{x}) - g(\underline{x})u + q_a - d(\underline{x},t) \tag{32}$$

Once $f(\underline{x})$ and $g(\underline{x})$ are known and $d(\underline{x},t)=0$, the idea controller is obtained through feed linearization as [15]:

$$u^{*}=g^{-1}(\underline{x})\left(-f(x)+q_{a}+Ks\right) \tag{33}$$

Where K>0 is a real constant. The assumptions of $f(\underline{x})$, $g(\underline{x})$ and x_d in (29) ensure that u* is bounded. The insertion of Eqs. (32) and (33) and simplifications yielded $\dot{s}+Ks=0$, which is a Hurwitz equation and leads to the convergence of the error function to zero. However, system dynamics is not always available in practice, and external disturbances worsen the performance of the system. Consequently, the ideal controller represented in Eq. (33) cannot be executed [5]. The real intelligent CRBENN controller introduced below incorporates $d(\underline{x},t)$ and uncertainties. Furthermore, a robust control term is added to the control scheme to mitigate external disturbance, $d(\underline{x},t)$, and approximation error.

C. Proposed Control Structure

The proposed CRBENN is employed in a direct adaptive control structure in order to approximate the ideal control rule u* in Eq. (33) in the form of $\hat{u}$. A general direct adaptive robust emotional neuro controller (DARENC) was designed as [5]:

$$u=u-\frac{u_{r}}{g(\underline{x})} \tag{34}$$

Where u_r denotes the resistant compensation term:

$$u_{r}=-\frac{1}{r}Ps \tag{35}$$

Where r is a positive constant, and $P=P^T$ is a positive semidefinite matrix. A unique solution to the following pseudo-Riccati equation is given for each Q [5]:

$$-2KP+Q+P\left(\frac{1}{\rho^{2}}-\frac{2}{r}\right)P=0 \tag{36}$$

Where $2\rho^{2}\geq r$.

The emotion-based control rule $\hat{u}$ is designed as [5]:

$$u=\sum_{j=1}^{m}V_{j}\varphi_{j}-\sum_{j=1}^{m}\omega_{j}\varphi_{j}=(V-\omega)^{T}\varphi \tag{37}$$

where $V=[V_1, \ldots, V_m]^T \in R^m$ and $W=[W_1, \ldots, W_m]^T \in R^m$ are the adaptive weight vectors of the amygdala and orbitofrontal cortex (OFC) nodes respectively, and $\varphi=[\varphi_1, \varphi_2, \ldots, \varphi_m]^T$ is the RBF basis function vector.

It is assumed that $\underline{x}$ and adaptive parameters V and W belong to compact sets $\Omega_{x}=\left\{\underline{x}\,\middle|\,\|x\|\leq M_{x}\right\}$, $\Omega_{fv}=\left\{V\,\middle|\,\|V\|\leq M_{v}\right\}$, and $\Omega_{fw}=\left\{W\,\middle|\,\|W\|\leq M_{w}\right\}$, respectively, where M_x, M_v, and M_w are positive constants [5]. The ideal parameters V* and W* are defined as [5]:

$$\left[V^{*}\quad \omega^{*}\right]=\arg\min\left[\sup\left\|u\left(\underline{x}/[V\quad \omega]\right)-u^{*}\right\|\right] \tag{38}$$

where u* is the ideal control law given in (33). The insertion of Eq. (34) into Eq. (32) yields Eq. (39) for S derivatives:

$$\dot{s}=-g(\underline{x})(\hat{u}-u^{*})-Ks+u_{r}-d \tag{39}$$

where K > 0 is a feedback gain, u_r is the robust compensation term from (35), and d represents external disturbances.

For unknown ideal parameters V* and W*, the minimum approximation error is defined as [5]:

$$\omega_{c}=-g(\underline{x})\left(u\left(\left(\underline{x}/[V\quad \omega]\right)\right)-u^{*}\right) \tag{40}$$

Where $\omega_{c}\in L_{\infty}$.

Based on Eqs. (38-40):

$$\dot{s}=-g(\underline{x})\tilde{v}^{T}\varphi-g(\underline{x})\tilde{w}^{T}\varphi-Ks+u_{r}+w_{c}-d \tag{41}$$

Where $\tilde{W}=W^{*}-W$ and $\tilde{V}=V^{*}-V$.

The amygdala weights can only increase [11]. Therefore, the following update rules are applied to the amygdala and OFC weights [5]:

$$\dot{v}=\alpha P\varphi g(\underline{x})\max(S,0) \tag{42}$$

$$\dot{w}=-\beta P\varphi g(\underline{x})s \tag{43}$$

Where $\alpha>0$ and $\beta>0$ are learning rates corresponding to the amygdala and OFC weights, respectively. The max operator in Eq. (42) generates the amygdala update rule using the constant basis non-reducing learning rules. Drawing on Barbalat's lemma [16], the error function s can be proved to asymptotically converge to zero. Figure 4 illustrates a schematic of the proposed DARENC.

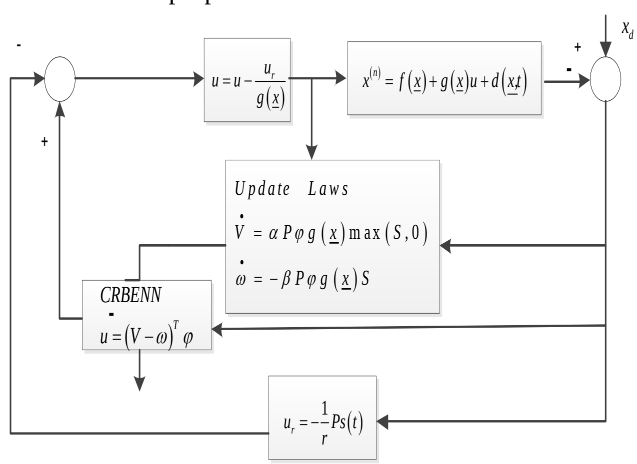

Fig. 4. Schematic view of DARENC [5]

Gaussian functions have many parameters to be tuned, e.g., Gaussian centers and their variances. The tuning of such parameters using adaptation rules would result in a heavy computational burden. To simplify the controller equations and implement universal approximation, the present work used Legendre functions rather than Gaussian ones.

According to the theorem of orthogonal functions, Legendre polynomials are orthogonal to each other, and an arbitrary function can be represented using a linear combination of such functions:

$$\varphi_{0}=1,\varphi_{1}=x,\varphi_{2}=\frac{(3x^{2}-1)}{2},x=\sin(\omega t) \tag{44}$$

Note 1: This study focused the design of CRBENN-based adaptive controllers. Hence, amygdala and OFC weights are adapted through the Lyapunov derivative rule of adaptation, while the RBF parameters (i.e., average and smoothing factors) are constant to simplify the calculations by reducing the number of adaptive parameters. In turn, there are fewer parameters to accelerate adaptation. In the simulation outputs, the RBF centers have the same distance in the input range, and the same smoothing factor is employed for all the Gaussian nodes. Constant parameters and the division of centers in the input range are common in neural network-based fuzzy or adaptive controllers [14].

Note 2: The unique adaptive control approach of this study is an example of using the CRBENN in the design of controllers. The CRBENN can be used in control or decision-making applications, e.g., system identification, prediction, and classification [5].

Note 3: To ensure the stability of the adaptive parameters, the update rules in Eqs. (42) and (43) were modified based on the image algorithm as [17]:

$$\dot{V}=\begin{cases}\alpha P\varphi g(\underline{x})\max(S,0) & if \quad \|V\|<M_v \quad or \\ (\|V\|=M_v \quad and \quad \alpha PV^T\varphi g(\underline{x})\max(S,0)\le 0) & \\ \alpha P\varphi g(\underline{x})\max(S,0)-\dfrac{\alpha PV^T\varphi g(\underline{x})\max(S,0)}{\|V\|^2}V & \\ if(\|V\|=M_v \quad and \quad \alpha PV^T\varphi g(\underline{x})\max(S,0)>0) & \end{cases} \tag{45}$$

$$\dot{W}=\begin{cases}-\beta P\varphi g(\underline{x})S & if \quad \|W\|<M_w \quad or \\ (\|W\|=M_w \quad and \quad \beta PW^T\varphi g(\underline{x})S\ge 0) & \\ -\beta P\varphi g(\underline{x})S+\dfrac{\beta PW^T\varphi g(\underline{x})}{\|W\|^2}W \quad if & \\ (\|W\|=M_w \quad and \quad \beta PW^T\varphi g(\underline{x})S<0) & \end{cases} \tag{46}$$

The above update rules make the adaptive parameters remain constrained. When the adaptive parameters are below their minimum bounds or are at their maximum bounds but approach smaller values, rules (45) and (46) change into ordinary rules (42) and (43). Hence, the second lines in Eqs. (45) and (46) hold only when the adaptive parameters are at their maximum values and approach larger values. The proof of Theorem 1 is discussed in [5].

Note 4: The computational complexity of the CRBENN is of an m×n-order, in which m is the number of RBFs in the thalamus, whereas n is the number of CRBENN inputs. Since the computational complexities of adaptive rules and control input are of an m-order, the computational complexity of DARENC is of an m×n×T_t-order, where $T_t=\left(\frac{1}{dt}\right)\times T$, T is the total execution time, and *dt* is the time step [5].

D. Simulation Results

An interconnected three-area power system was utilized to evaluate the effectiveness of DARENC shown in Fig. 5. Areas 1 and 2 have gas turbines (a single cycle and a combined cycle) and steam turbines, while Area 3 only has gas turbines. Table 2 reports the system parameters. It is a real-life three-area power system on the Persian Gulf coast. Area 1 has 56 stations with total output power of 4797 MW, Area 2 has 88 generation stations with a total capacity of14000 MW, and Area 3 has 28 stations with a total output power of 923 MW.

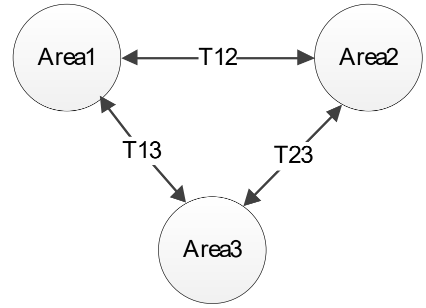

Fig. 5. Three-area power system

The load disturbance of each area is represented by a step function. The simulation results were compared for PSO-optimized PID, standard ENN, and DARENC parameters for each area.

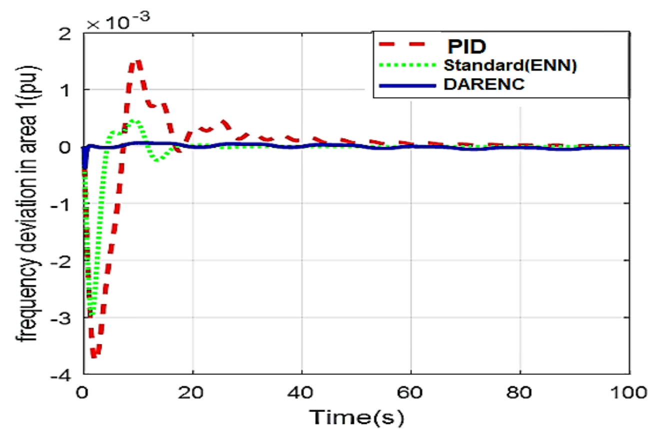

Fig. 6. Frequency control comparison of DARENC, standard ENN, and PID models in Area 1

The cost function for the optimization of the coefficients of the controllers was defined as:

$$\cos tfunction=\int(|\Delta f_1|+|\Delta f_2|+|\Delta f_3|)dt \tag{47}$$

Three scenarios were simulated for a reference signal of y_{mi}=0. Tables 3-5 provide the parameters of the PID controller, standard ENN, and DARENC, respectively.

TABLE I. Parameters of the power system areas

Parameter	Area 1	Area 2	Area 3
D_i	0.24	0.11	0.046
K_{ri}	0.3	0.3	
M_i	167	89.5	23.25
R_i	0.04	0.04	0.04
T_{t1i}	0.4	0.4	0.1
T_{g1i}	0.1	0.1	0.4
T_{t2i}	1.0	0.1	
T_{g2i}	0.1	0.1	
T_{ri}	1.0	1.0	
T_{ij}	T_{12}=8.4	T_{23}=1.5	T_{31}=1.5

TABLE II. DESCRIPTION OF PARAMETERSof the power system

Parameter	Description
ΔF_i	Frequency deviation
ΔP_{t1i}	Gas turbine power deviation
ΔP_{g1i}	Governor power deviation (gas turbine)
ΔP_{g2i}	Steam turbine power deviation
ΔP_{ri}	Steam heater power deviation
ΔP_{g2i}	Governor power deviation (steam turbine)
ΔP_{tie}	Power network connection line deviation
D_i	Load damping coefficient
K_{ri}	Heater gain
M_i	Inertia constant
R_i	Governor speed adjustment
T_{t1i}	Gas turbine time constant
T_{g1i}	Governor time constant
T_{t2i}	Steam turbine time constant
T_{g2i}	Governor time constant
T_{ri}	Heater time constant
T_{ij}	Synchronization power constant

TABLE III. PID CONTROLLER PARAMETERS

area	K_p	K_d	K_i
1	0.0413	0.0981	0.0981
2	0.0839	0.0581	0.0581
3	0.0471	0.0326	0.0326

TABLE IV. STANDARD ENN PARAMETERS

area	K_p	K_d	R	ω	β	α
1	4.3612	0.0703	0.5078	0.7250	27.5855	0.7896
2	0.0540	0.0255	3.3975	0.9912	0.2827	0.4694
3	0.8960	0.6799	0.0684	0.6849	0.7286	0.3090

TABLE V. DARENC PARAMETERS

	area1	area 2	area 3
K_p	0.0058	0.0259	0.1365
K_d	87.4358	78.6028	17.0263
α	0.8699	0.8408	0.8397
β	3.8651	2.2346	0.2264
ω	0.3761	0.0060	0.0287
p	24.9756	5.6056	0.0730
r	0.7982	2.1916	0.7688

In the first scenario, a load disturbance of 500 MW (0.5 pu) was assumed in Area 1. Figures 6 and 7 demonstrate the simulation results. Figure 6 depicts the frequency variation for the steady-state error of zero in Area 1 with a load change. Accordingly, DARENC led to a lower frequency variation than the standard ENN and PID controllers. The cost function, which is the sum of the absolute integral of the frequency variations of the three areas, was found to be 0.0684, 0.0212, and 0.0057 for the PID, standard ENN, and DARENC models, respectively. Figure 7 depicts the connection line power variations in the areas. As can be seen, the controllers showed the same power control performance as frequency control.

In the second scenario, Areas 1-3 were assumed to have load changes of 0.4, 0.3, and 0.05 pu, respectively, as shown in Figs. 8 and 9. Figure 8 demonstrates the frequency variations of the three areas for all the controllers at the zero steady-state error.

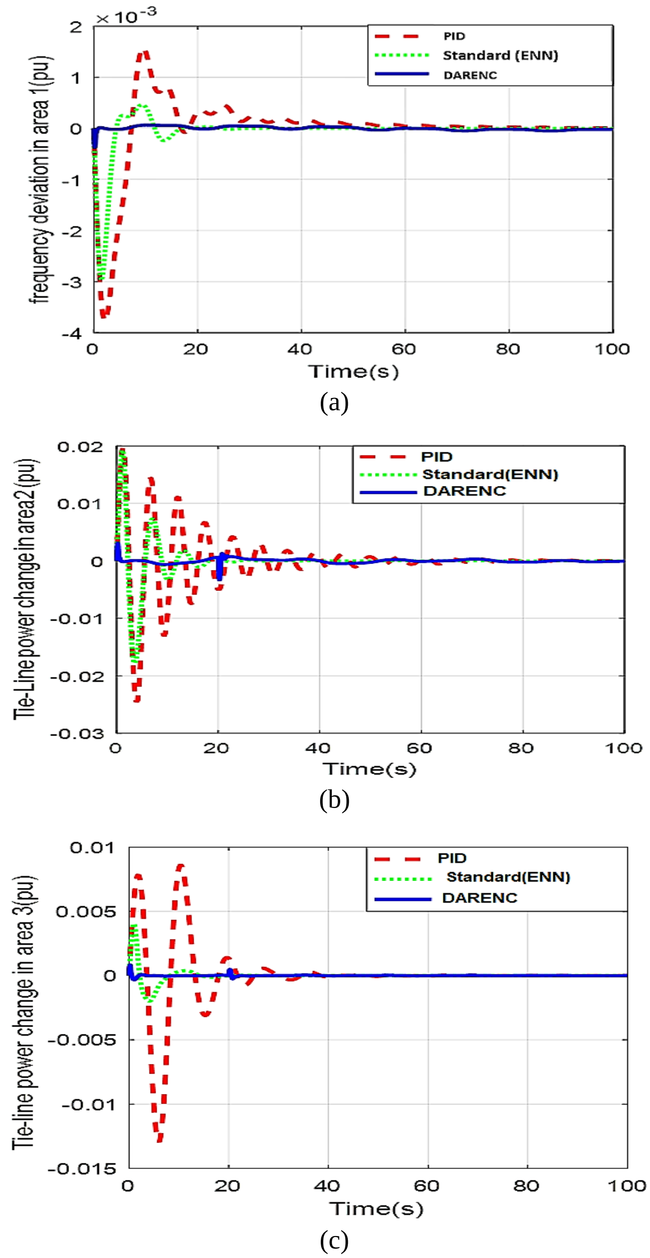

Fig. 7. Power control comparison of the PID, standard ENN, and DARENC models for Area1(a), Area2 (b), and Area3 (c)

According to Fig. 8, DARENC led to lower frequency variations than the standard ENN and PID controllers. The cost function was calculated to be 0.06807, 0.0874, and 0.00282 for the PID, standard ENN, and DARENC models, respectively. Figure 9 plots the connection line power variations of the three areas. As can be seen, the controllers showed the same power control performance as frequency control.

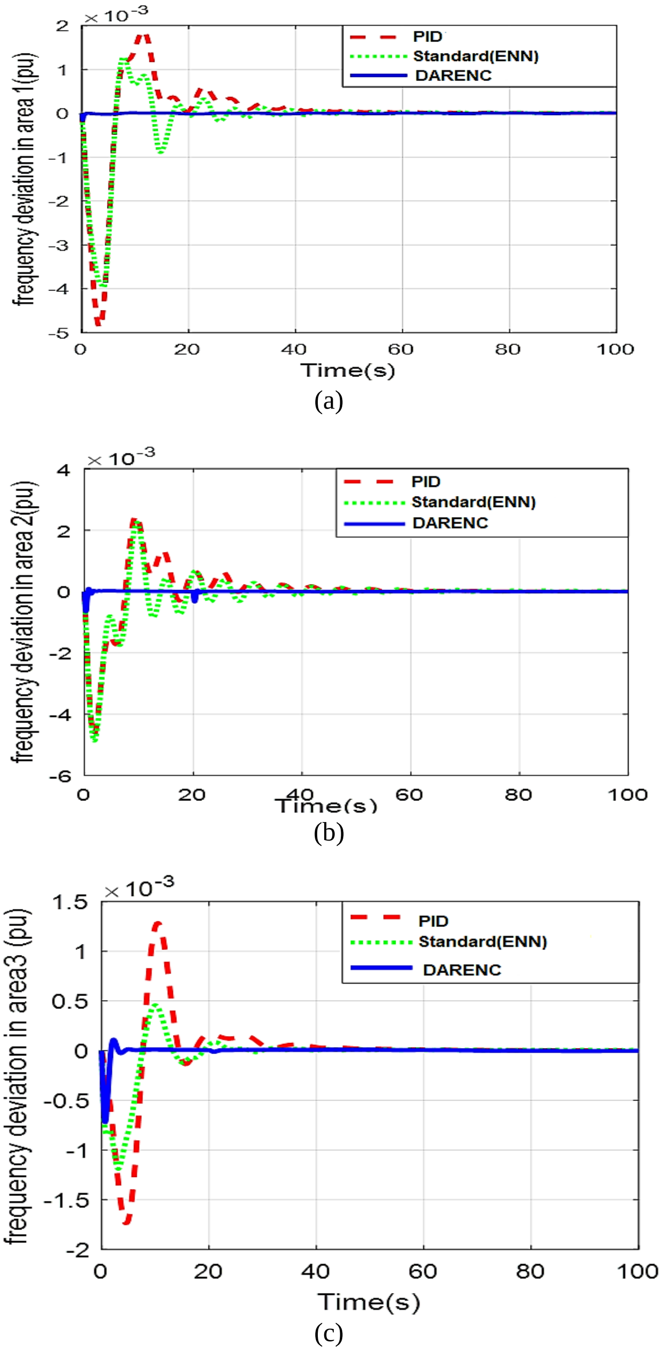

Fig. 8. Frequency control comparison of DARENC, PID, and standard ENN models for Area1(a), Area2 (b), and Area3 (c)

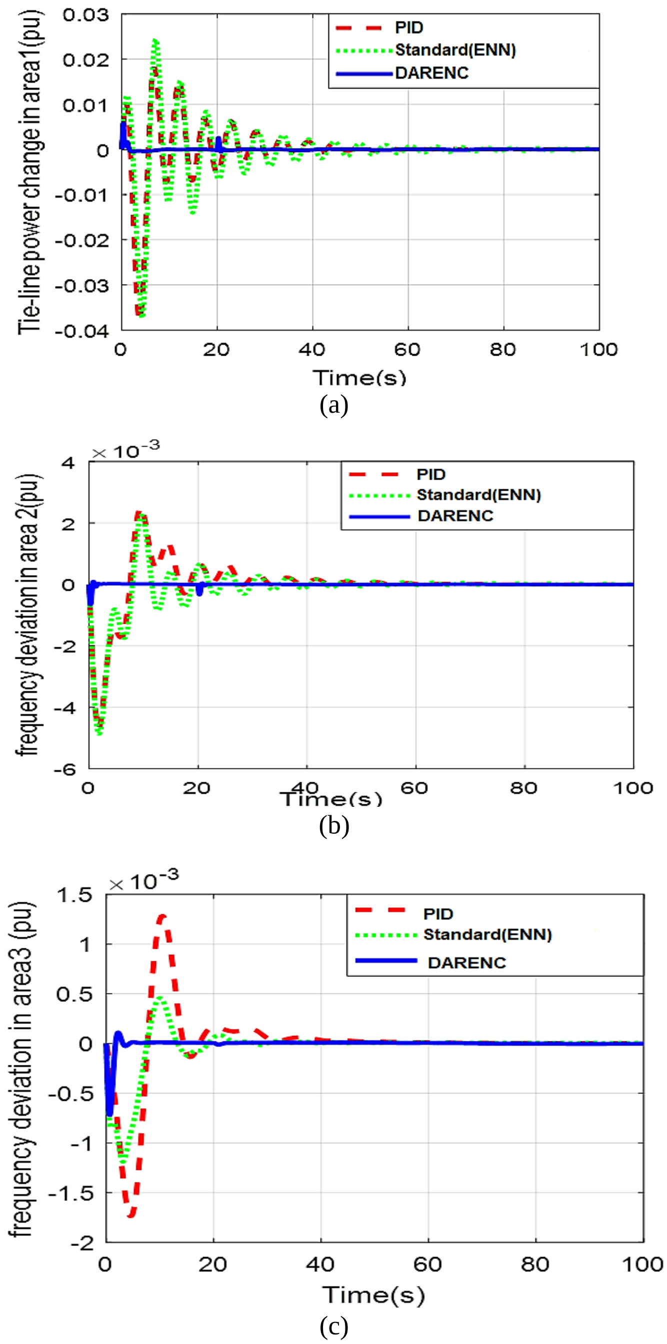

Fig. 9. Power control comparison of DARENC, PID, and standard ENN models for Area1(a), Area2 (b), and Area3 (c)

In the third scenario, the performance of the controllers under sudden load changes was evaluated. Figure 10 plots the load change. A sudden load change was applied to the system at t=10 s, and the system was restored in all three areas at t=30 s.

According to Fig. 11, DARENC model had a lower frequency fluctuation than the PID and standard ENN controllers. The PID, standard ENN, and DARENC models were found to have a cost function of 0.03679, 0.08858, and 0.004918, respectively. According to Fig. 11, once a sharp load change occurred, the PID controller outperformed the standard ENN controller.

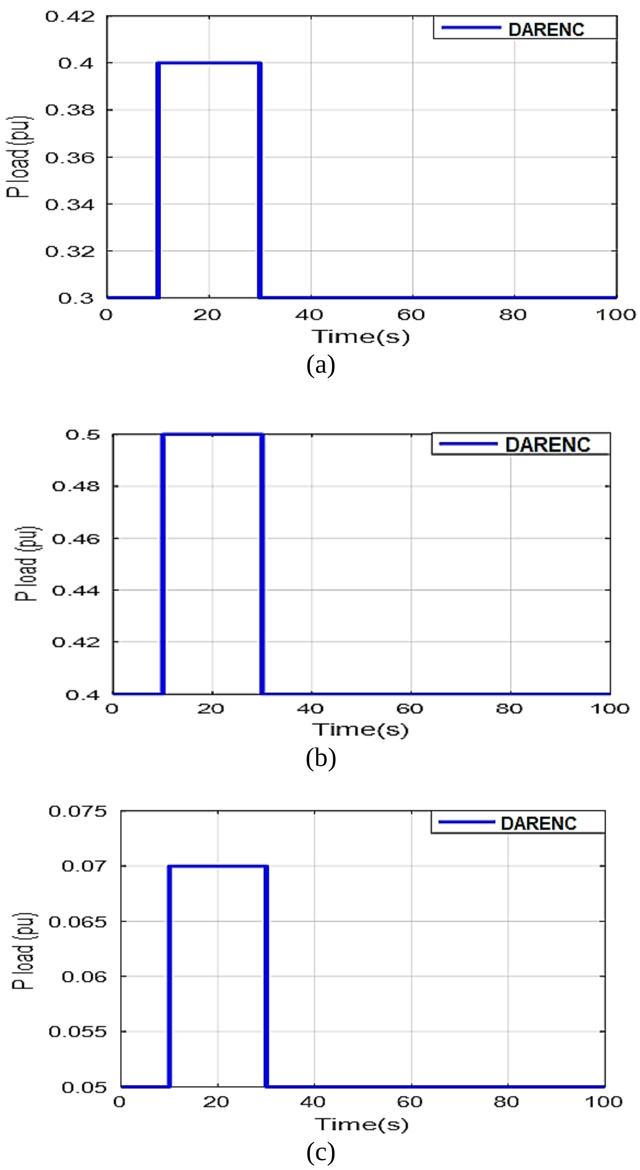

Fig. 10. Load change in Area1(a), Area2 (b), and Area3 (c)

The maximum frequency variation is a crucial factor in power systems. Table X reports the maximum frequency variations of the three areas under the three scenarios. According to Table 6, the frequency deviation of the PID controller was larger than those of the standard ENN and DARENC models, and DARENC model outperformed the PID and standard ENN models.

TABLE VI. FREQUENCY DEVIATION VS. TIME FOR DARENC, STANDARD ENN, AND PID MODELS

area	PID	standard ENN	DARENC
1	0.5	0.3	0.028
2	0.5	0.3	0.07
3	0.2	0.1	0.07

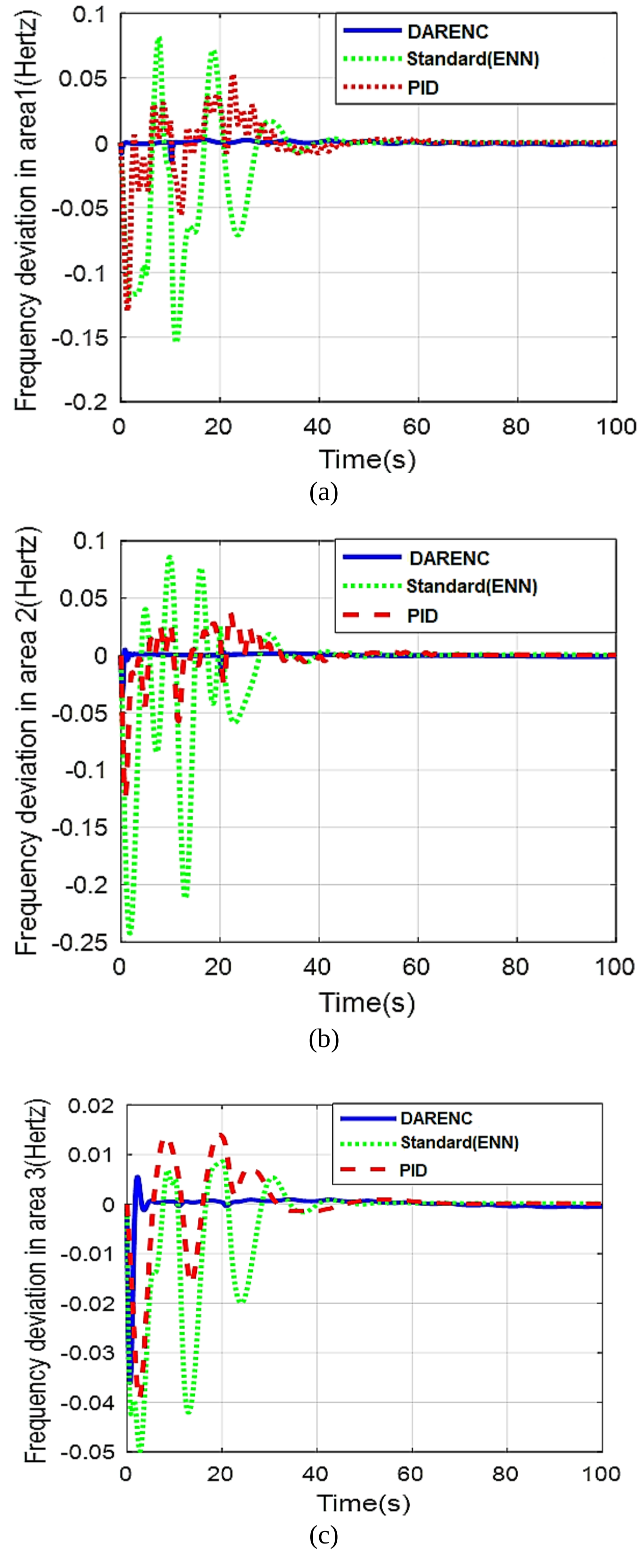

Fig. 11. Frequency control comparison of DARENC, PID, and standard ENN models in Area1(a), Area2 (b), and Area3 (c)

IV. CONCLUSION

This paper proposed a novel load frequency controller for multi-area power systems with unknown parameters. The proposed controller was developed by integrating BEL into the Lyapunov function and PSO. For this purpose, PSO was employed to optimize the BEL coefficients, whereas the Lyapunov function was adopted to stabilize its response. The proposed controller achieves LFC objectives in the presence of uncertainties. It also reduced the approximation error and the effects of external disturbance on tracking performance using an auxiliary control signal. A combined Lyapunov function was employed to represent the tracking error frontier of the closed-loop system and parameter error. A three-area power system was adopted for the validation of the proposed model. The simulations indicated that the proposed controller could achieve LFC objectives in terms of the zero steady-state error frequency and tie-line deviations in power system areas, while each area managed its load demand. The proposed controller proved to be advantageous over PID and standard ENN controllers.

V. REFERENCES

[1] P. S. Kundur and O. P. Malik, Power system stability and control. McGraw-Hill Education, 2022.

[2] W. Tan, “Load frequency control: Problems and solutions,” in proceedings of the 30th Chinese control conference, 2011, pp. 6281–6286.

[3] R. L. Williams, D. A. Lawrence, and others, Linear state-space control systems. John Wiley & Sons, 2007.

[4] H. Yousef, “Adaptive fuzzy logic load frequency control of multi-area power system,” Int. J. Electr. Power Energy Syst., vol. 68, pp. 384–395, 2015.

[5] F. Baghbani, M.-R. Akbarzadeh-T, M.-B. Naghibi-Sistani, and A. Akbarzadeh, “Emotional neural networks with universal approximation property for stable direct adaptive nonlinear control systems,” Eng. Appl. Artif. Intell., vol. 89, p. 103447, 2020.

[6] K. Hornik, M. Stinchcombe, and H. White, “Multilayer feedforward networks are universal approximators,” Neural networks, vol. 2, no. 5, pp. 359–366, 1989.

[7] J. L. Castro, “Fuzzy logic controllers are universal approximators,” IEEE Trans. Syst. Man. Cybern., vol. 25, no. 4, pp. 629–635, 1995.

[8] C. Lucas, D. Shahmirzadi, and N. Sheikholeslami, “Introducing BELBIC: brain emotional learning based intelligent controller,” Intell. Autom. Soft Comput., vol. 10, no. 1, pp. 11–21, 2004.

[9] J. J. Moren, “Emotion and learning: A computational model of the amygdala.,” 2004.

[10] F. Baghbani, M.-R. Akbarzadeh-T, and M.-B. N. Sistani, “Stable robust adaptive radial basis emotional neurocontrol for a class of uncertain nonlinear systems,” Neurocomputing, vol. 309, pp. 11–26, 2018.

[11] J. Morén and C. Balkenius, “A computational model of emotional learning in the amygdala,” From Anim. to Animat., vol. 6, pp. 115–124, 2000.

[12] Y.-C. Hsueh, S.-F. Su, C.-W. Tao, and C.-C. Hsiao, “Robust L_2-Gain Compensative Control for Direct-Adaptive Fuzzy-Control-System Design,” IEEE Trans. Fuzzy Syst., vol. 18, no. 4, pp. 661–673, 2010.

[13] Y.-C. Hsueh and S.-F. Su, “Learning error feedback design of direct adaptive fuzzy control systems,” IEEE Trans. Fuzzy Syst., vol. 20, no. 3, pp. 536–545, 2011.

[14] Y. Pan, H. Yu, and M. J. Er, “Adaptive neural PD control with semiglobal asymptotic stabilization guarantee,” IEEE Trans. Neural Networks Learn. Syst., vol. 25, no. 12, pp. 2264–2274, 2014.

[15] J.-J. E. Slotine, W. Li, and others, Applied nonlinear control, vol. 199, no. 1. Prentice hall Englewood Cliffs, NJ, 1991.

[16] M. Ott, M. AlMuhaini, and M. Khalid, “A MILP-Based Restoration Technique for Multi-Microgrid Distribution Systems,” IEEE Access, vol. 7, pp. 136801–136811, 2019, doi: 10.1109/access.2019.2942633.

[17] L.-X. Wang, A course in fuzzy systems and control. Prentice-Hall, Inc., 1996.

[18] S. M. Abd-Elazim and E. S. Ali, “Load frequency control of a multi-area multi-source power system using Henry gas solubility optimization,” IEEE Access, vol. 10, pp. 10146–10156, 2022.

[19] A. K. Barik and D. C. Das, “Load frequency control of a renewable energy based isolated microgrid using brain emotional learning based intelligent controller,” Electric Power Systems Research, vol. 212, p. 108278, 2022.

[20] M. Kheradmandi, P. Ahmadi, and A. R. Ghaffari, “A robust adaptive load frequency control based on improved brain emotional learning algorithm,” IET Generation, Transmission & Distribution, vol. 14, no. 15, pp. 2992–3001, 2020.

[21] J. Liu, Y. Zhang, and H. Wang, “Brain Emotional Learning-Based IntelligentControl for Power System Frequency Regulation: A Comprehensive Review,”IEEE Transactions on Industrial Informatics, vol. 18, no. 5, pp. 3456–3468, 2022.